SCIENCE CHINA

Technological Sciences

July 2010 Vol.53 No.7: 1983–1992 doi: 10.1007/s11431-010-3226-y

Characteristic analysis of unsteady viscous flow around a cavitating propeller

ZHU ZhiFeng^{1, 2*}, FANG ShiLang¹ & WANG XiaoYan¹

¹ Key Laboratory of Underwater Acoustic Signal Processing of Ministry of Education, Southeast University, Nanjing 210096, China;
² School of Electrical Engineering and Information, Anhui University of Technology, Maanshan 243002, China

Received December 24, 2009; accepted April 19, 2010

Based on viscous multiphase flow theory, this paper presents some recent validation results with a hybrid grid and sliding mesh solving Unsteady Navier-Stokes (N-S) and Bubble Dynamics equations as applied to prediction of pressure, velocity and vapor volume fraction in the wake in an uniform inflow. Comparable to experimental results, numerical predictions of sheet cavitation, tip vortex cavitation and hub vortex cavitation are in agreement with the corresponding experimental data, the same as numerical predictions of pressure in wake. Tip vortex cavitation is the most important to generate the pressure fluctuation within the near wake. The characteristics such as blade and shaft rate frequency of propeller pressure in wake coincide with its geometric model and parameters. With increasing distance from propeller disk, the pressure signals at blade frequency decrease. The process of attenuation becomes fast with the decreased advance coefficient and cavitation number.

cavitating flow, RANS, propeller, sliding mesh, multiphase flow

Citation:

Zhu Z F, Fang S L, Wang X Y. Characteristic analysis of unsteady viscous flow around a caviatating propeller. Sci China Tech Sci, 2010, 53: 1983–1992, doi: 10.1007/s11431-010-3226-y

1 Introduction

The propeller cavitation not only degrades hydrodynamic performance on propeller, results in cavitation erosion and induces hull vibration but also causes enough cavitation noise to expose them. The noise and hull vibration induced by propeller strictly relate to cavitating flow, pressure and wake structure. Therefore, acquiring much information of flow field about cavity, pressure and so on plays an important role in understanding the forming mechanism of propeller vibration and noise. This is very helpful for us to not only analyze noise characteristics but also reduce noise and vibration.

At present, the cavitating flow is studied mainly by ex-

periment in cavitation tunnel and numerical simulation. Experiment can show wake characteristics accurately, but it is costly and time consuming. Numerical method has more information of flow field, but grid, turbulence model, cavitation model and their parameters may make the computed results unstable. Therefore, the reliable numerical studies of the wake require corresponding experimental data. In 1979, MIT's Lee [1] began to study propeller cavitation using lifting surface theory. Ship scientific research center and universities [2–4] in China studied propeller hydrodynamic performance and cavitation with theoretical, numerical and experimental methods. For study on fluctuating cavitation volume and the unstable jet during bubbles collapse, viscid-flow theory is more advanced for not requiring bubbles shape and bubbles collapse model in advance. At present, numerical simulation based on viscid-flow theory is becoming more and more perfect. It can simulate accurately

^{*}Corresponding author (email: zzf@ahut.edu.cn)

pressure and velocity distribution in wake field of propeller and water turbine as well as cavitation of hydrofoil and revolution body. Using sliding mesh, refs. [5, 6] numerically investigated propulsion of podded propeller driven ship and fluctuating pressure of turbine, and simulated three-dimensional unsteady turbulence in full passage with RNG k- ε turbulence model. However, there was no cavitation in their studies. Based on multi-phase model, ref. [7] numerically simulated unsteady flow around hydrofoils using CFD code (FLUENT). The numerical prediction of cavity length, the velocity field inside and outside of the vapor cavity and the pressure coefficient agrees with experimental results. Nevertheless, the propeller cavitation was not involved furthermore. Due to mass transport between phases in cavitation flow, the feature of unsteady-state and high Reynolds number in wake, it is very difficult to make the numerical prediction of cavitating flow around propeller. For propeller cavitating flow study, there are only few literatures published which were based on steady computation. A three-dimensional, multiphase Reynolds-Averaged Navier-Stokes (RANS) solver was applied to propeller load breakdown, due to cavitation by Lindau [8] from the Pennsylvania State University. The cavitation size and shape as well as breakdown behavior are in agreement with the measured data. Cavitation of propeller blade using an unstructured grid and k-ω turbulence model based on Navier-Stoker solver was studied by Kawamura [9] from University of Tokyo. The water performance, cavitation inception and cavitation shape are in good agreement with the well-known experimental measurements and observation. However, there was no tip vortex cavitation and hub vortex cavitation appearing in the two computational results. The vortex cavitation has important influence on the high frequency range of cavitation noise, so it is particularly predicted in the paper. Otherwise, ref. [10] experimentally investigated the feature of fluctuating pressure in wake, but did not study the influence of cavitation number on it. It also made numerical prediction of the fluctuation pressure which is seldom reported in literature, and some active results were obtained.

Based on viscid-flow and multiphase-flow theories, this paper adopts full cavitation model [11], turbulence model and sliding mesh to numerically solve unsteady N-S equations applied in 3D propeller caviting flow field. Compared with the corresponding measured results, the numerical predictions of propeller sheet, hub vortex and tip vortex cavitations were investigated to validate the numerical approach used in the paper. Then, computations were performed to analyze the evolution of pressure signals at four radial and four longitudinal positions downstream the propeller model at different advance and cavitation numbers. The characteristics of the spectrum of the pressure signals modulated by the propeller were also analyzed.

2 Mathematical modeling

Based on viscous flow and mixture multiphase flow model, the N-S Solver defining a density field is suitable for three-dimensional unsteady flow analysis. Phase change rates introduce cavitation model to vapor-water two-phase mixture flow model, which involves the interaction and slip velocity between the two phases. On the assumption that the flow field consists of vapor and water whose densities are constant, the vapor-water two-phase flow is taken as a mixture flow whose total variable density is the function of vapor volume fraction. On the one hand, the quantities of mixture flow expressed by means of vapor and water volume fraction are solved by N-S equation. On the other hand, vapor transport equation is adopted to solve vapor volume fraction. The mixture flow is taken as a flow, and then the governing equations can be written as the mass and momentum conservation of the mixture flow, such that

$$\frac{\partial}{\partial t}(\rho_{\rm m}) + \frac{\partial}{\partial x_j}(\rho_{\rm m}u_{\rm mj}) = 0, \qquad (1)$$

$$\frac{\partial}{\partial t}(\rho_{m}u_{mi}) + \frac{\partial}{\partial x_{j}}(\rho_{m}u_{mi}u_{mj}) = -\frac{\partial p}{\partial x_{i}} + \frac{\partial}{\partial x_{j}}(\alpha_{v}\rho_{v}u_{d,vi}u_{d,vj})
\times \frac{\partial}{\partial x_{j}}\mu_{m} \left[\left(\frac{\partial u_{mi}}{\partial x_{j}} + \frac{\partial u_{mj}}{\partial x_{i}} \right) - \frac{2}{3}\delta_{ij}\frac{\partial u_{mk}}{\partial x_{k}} \right],$$
(2)

where subscripts m, v and 1 correspond to mixture, vapor and water respectively. $u_{\rm mi}=(\alpha_{\rm l}\rho_{\rm l}u_{\rm li}+\alpha_{\rm v}\rho_{\rm v}u_{\rm vi})/\rho_{\rm m}$ is mass averaged-velocity, $\rho_{\rm m}=\alpha_{\rm l}\rho_{\rm l}+\alpha_{\rm v}\rho_{\rm v}$ is the mixture viscosity, $\mu_{\rm m}=\alpha_{\rm l}\mu_{\rm l}+\alpha_{\rm v}\mu_{\rm v}$ is the mixture viscosity and $u_{\rm d,vi}=u_{\rm vi}-u_{\rm mi}$ is the drift velocity for the vapor phase.

Rates of vapor generation and condensation (R_c and R_e) introduce cavitation model [11]. When pressure $p < p_v$ (vapor pressure), liquid phase becomes vapor phase and bubbles appear. The increase amount of vapor phase is equal to the decrease amount of liquid. Vapor and liquid phases transport equations are written as

$$\frac{\partial}{\partial t} (\alpha_{v} \rho_{v}) + \frac{\partial}{\partial x_{i}} (\alpha_{v} \rho_{v} u_{vj}) = R_{e}, \tag{3}$$

$$\frac{\partial}{\partial t} \left[(1 - \alpha_{v}) \rho_{1} \right] + \frac{\partial}{\partial x_{i}} \left[(1 - \alpha_{v}) \rho_{1} u_{1i} \right] = -R_{e}, \tag{4}$$

where R_e is vapor generation rate. Combining eqs. (3) and (4) yields eq. (1).

From derivative of $\rho_{\rm m}$ for mixture density expression, we obtain

$$\frac{D\rho_{\rm m}}{Dt} = -(\rho_{\rm l} - \rho_{\rm v}) \frac{D\alpha_{\rm v}}{Dt}.$$
 (5)

The vapor volume fraction $\alpha_{\rm v}$ relates to the bubble num-

ber density n_b and bubble radius R_b as $\alpha_v = \frac{4}{3}n_b\pi R_b^3$ which is substituted into eq. (5) to obtain

$$\frac{D\rho_{\rm m}}{Dt} = -(\rho_{\rm l} - \rho_{\rm v}) (n_{\rm b} 4\pi)^{1/3} (3\alpha_{\rm v})^{2/3} \frac{DR_{\rm b}}{Dt}.$$
 (6)

The bubble dynamics equation can be derived from the general Rayleigh-plesset equation as [12,13]

$$R_{\rm b} \frac{{\rm d}^2 R_{\rm b}}{{\rm d}t^2} + \frac{3}{2} \left(\frac{{\rm d}R_{\rm b}}{{\rm d}t} \right)^2 = \frac{p_{\rm v} - p - 2\gamma / R_{\rm b} - 4(\mu_{\rm l} / R_{\rm b})({\rm d}R_{\rm b} / {\rm d}t)}{\rho_{\rm l}}. (7)$$

From eqs. (1), (3), (5), (6) and (7), we get

$$R_{e} = \frac{3\alpha_{v}}{R_{b}} \frac{\rho_{v} \rho_{l}}{\rho_{m}} \left(\frac{2}{3} \frac{p_{v} - p}{\rho_{l}} - \frac{2}{3} R_{b} \frac{D^{2} R_{b}}{D t^{2}} \right)^{1/2}.$$
 (8)

According to the nuclear industry [14], when the volume of bubbles increases R_b is commonly expressed as $R_b = C \frac{\gamma}{\rho_1 v^2}$, where v is relative velocity between liquid

and vapor phase, γ is surface tension coefficient and C is constant. R_b is determined by turbulent fluctuation pressure and surface tension forces. Here, the relative velocity is substituted by turbulent velocity for their close values. Because vapor generation rate is in proportion to liquid mass fraction $(1-f_v)$, we ignore derivative of second order and substitute turbulence kinetic energy k for v^2 , and then obtain the net phase change rate as

$$R_{e} = Ce \frac{k}{\gamma} \rho_{1} \rho_{v} \sqrt{\frac{2}{3} \frac{p_{v} - p}{\rho_{1}}} (1 - f_{v}).$$
 (9)

When pressure $p>p_v$, vapor phase becomes liquid phase. In the same way, we obtain net vapor condensation rate R_c as

$$R_c = Cc \frac{k}{\gamma} \rho_1 \rho_v \sqrt{\frac{2}{3} \frac{p - p_v}{\rho_1}} f_v , \qquad (10)$$

where vapor mass fraction is expressed by $f_v = \alpha_v \rho_v / \rho_m$, and Ce=0.02 Cc=0.01 are two empirical constants [11]. According to ref. [11], vapor condensation rate was found to be in proportion to the square root of local turbulent kinetic energy \sqrt{k} in hydrofoil experiment, and then \sqrt{k} is substituted for k in eqs. (9) and (10). However, here propeller is different from hydrofoil, so according to dimension analysis k is adopted in eqs. (9) and (10). The models were modified by User Define Function (UDF) in FLUENT to realize numerical computation. The cavitation model was introduced to computational code through phase change rate Re modified by UDF.

Being Reynolds-Average processed, the N-S equation (4) turns into RANS that becomes governing equation of aver-

age quantities in flow field. There is a Reynolds stress $\frac{\partial}{\partial x_i} \left(-\rho_m \overline{u'_{mi} u'_{mj}} \right)$ on the right of the equation, which ex-

presses the effect of turbulence. Based on Boussinesq assumption, we obtain

$$\frac{\partial}{\partial x_{j}} \left(-\rho_{m} \overline{u'_{mi} u'_{mj}} \right)
= \frac{\partial}{\partial x_{j}} \left[\mu_{t} \left(\frac{\partial u_{mi}}{\partial x_{j}} + \frac{\partial u_{mj}}{\partial x_{i}} \right) - \frac{2}{3} \left(\mu_{t} \frac{\partial u_{mi}}{\partial x_{j}} + \rho_{m} k \right) \delta_{ij} \right].$$
(11)

The k- ω turbulence model is suitable for different kinds of grids, but RNG k- ε [15,16] turbulence model is adept at prediction of viscous flow around wall. Computational results indicate that the parameter $C_{1\varepsilon}$ in ε equation is set as 1.47 to enhance prediction accuracy of sheet structure in propeller wake. In addition, according to ref. [17] turbulent viscosity coefficient μ_t modified by the form: $\mu_t = [\rho_v + \alpha_v^n(\rho_l - \rho_v)]C_\mu k^2/\varepsilon$, $C_\mu = 0.085$, n = 2, can improve modeling of the unsteady sheet cavitation. The computational results show that the correctional full cavitation model and the RNG k- ε turbulence model with modified parameters improve prediction accuracy of tip vortex cavitation, which contributes to characteristic analysis of pressure in wake.

3 Numerical method

In the paper, a four-blade skewed propeller E779A was selected for the reason that it had been widely studied in laboratory, and much reliable measurement data had been collected. The detailed parameters geometric model of E779A can be found in ref. [18]. Due to complicated shape of propeller blade, it is difficult to generate directly three-dimensional geometric model in the FLUENT preprocessors GAMBIT. Therefore, the model was finished by professional modeling tools UG, and then introduced to GAMBIT.

The computational domain is a full passage like cylinder around propeller. Considering the feasibility and computational efficiency, the domain was meshed by hybrid grid strategy. Due to skewed propeller blades, flow field near the propeller was meshed by unstructured grid with smaller triangles. The number of cells of the unstructured grid near the propeller is 614241. The velocity around tip is higher, so the density of the grid became larger from hub to tip. The number of cells of structured grid in outer field is 1318950. There is relative rotation between flow fields close to propeller and far away from propeller in the computational domain. The grids in the two fields are connected through grid interface along which the two grids slip relatively. Therefore sliding mesh was adopted to simulate the unsteady flow, which varies periodically in the rotation machine. The upstream inlet boundary in the computational domain is steady velocity-inlet whose number is equal to

that of axial free stream velocity. The downstream outlet boundary is set as a pressure-outlet, which is the same as reference pressure. The velocity of the outer boundary is the same as that of inlet boundary.

4 Results

In the following sections, the advance ratio J and the cavitation number σ_n of propeller are defined respectively by $J=U_{\infty}/(2nR)$ and $\sigma_n=(p_{\infty}-p_{\rm v})/(2\rho_1n^2R^2)$ where U_{∞} is inlet velocity, n is the propeller revolution speed, the propeller radius R=0.1136 m and p_{∞} is the reference pressure. The values of σ_n are varied by adjusting p_{∞} . Keep n equal to 25 r/s and change U_{∞} to get different J. In addition, the propeller hydrodynamics performance has been studied in other paper [19].

4.1 Numerical results and analysis of propeller cavitation

Sheet cavitation and vortex caivtation are very important and strictly related to water performance breakdown and noise. Therefore, the numerical prediction at J=0.71, $\sigma_n=$ 1.515 condition was compared with the measured data [20]. Cavitation shape, expressed by vapor volume fraction, and pressure distribution on backside of propeller blade at J=0.71 $\sigma_v = 1.515$ and $Re = 1.29 \times 10^6$ condition are shown in Figures 1(a) and 1(b) respectively. Reynolds number is expressed by $Re = nD^2/v_1$, where v_1 is kinematic viscosity factor. Red regions in Figure 1(a) mean vapor, expressing strong cavitation. On the contrary, blue regions mean weak cavitation. The plot illustrates that the cavitation appears in leading edge and tip regions, named leading edge and tip cavitation. The hub vortex cavitation at the center of the hub is well predicted due to its fine grid, as shown also in Figure 1(a). According to the comparison of Figures 1(a) and 1(b), it is found that the high vapor volume fraction area closely matches the low-pressure area. At the same time, it is noted that the pressure coefficient $Cp=(p-p_{\infty})/[2\rho_1(nR)^2]$ is maintained constantly at $-1.51(-\sigma_n)$ in the tip cavitating area where pressure is the lowest at p=2368 Pa, as expected from the common cavitation theory. The propeller rotates in an anticlockwise direction from inflow view. Figures 2(a) and

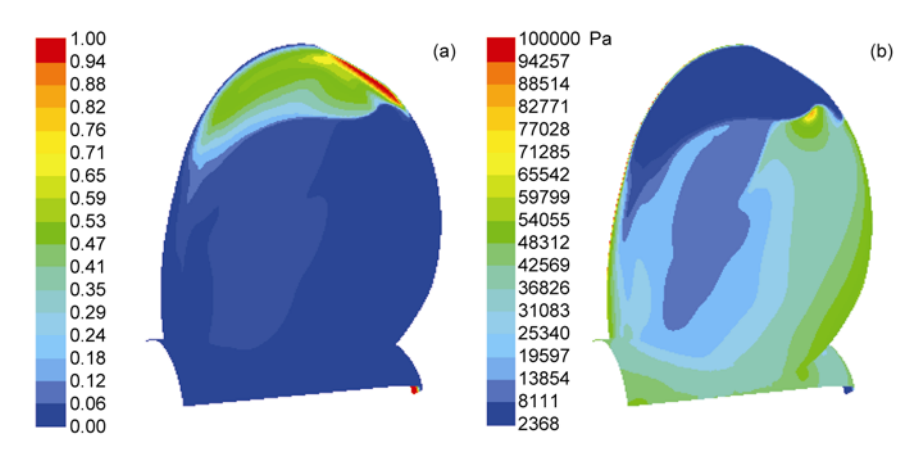


Figure 1 Numerical results on the back surface of blade at J=0.71, $\sigma_n=1.515$. (a) The distribution of vapor volume fraction; (b) pressure distribution.

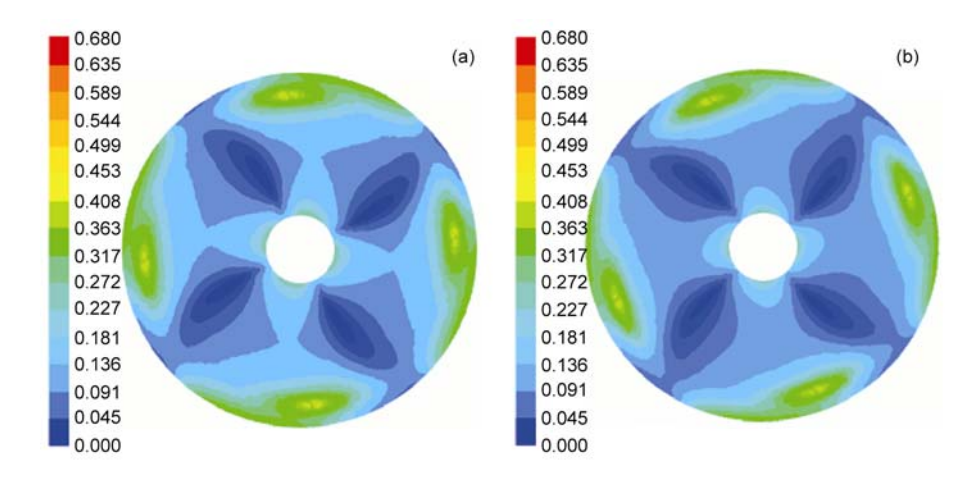


Figure 2 Numerical results of tip vortex cavitation in transversal planes of x/R=0.1. (a) The distribution of vapor volume fraction at time t=0 s; (b) the distribution of vapor volume fraction at time t=0.002 s.

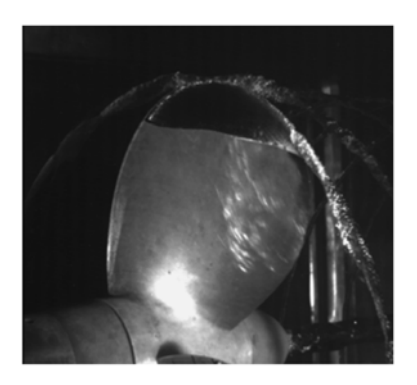


Figure 3 Experimental photograph of propeller E779A cavitation [20].

2(b) are the contours of cavitation in downstream direction approximately at x/R=0.1 transversal plane at the time of 0 s and 0.02 s respectively. According to the comparison of the two figures, the yellow bright pots located at r/R=0.9 in the two planes are tip vortex cavitation shed from blade trailing edge, and the cavitation rotates anticlockwise from inflow direction, coinciding with propeller rotation. Photograph in Figure 3 [20], captured by high-velocity camera through sealed window, shows the sheet and tip vortex cavitation at J=0.71 and σ_n =1.515. It is clearly seen from comparison of Figures 3, 1 and 2 that the numerical results of sheet and vortex cavitation accord with experiment.

4.2 Characteristic analysis and numerical results of unsteady pressure in wake

In this section, the correlation between fluctuating pressure and wake structures is investigated. The total pressure is equal to Static pressure plus Dynamic pressure. The time step in the paper was set up to 1 ms, so the grid rotates 9° per time step. Because pressure around tip vortex in the wake close to the propeller varies obviously and the feature of frequency is clear, the pressure fluctuation and the relationship with J are investigated using position at x=0.5R, r=0.9R. Pressures evolutions in different J conditions at the position are shown in Figure 4. Every wave shape indicates

that there appear four peaks in one period (0.04 s) and there are 90 degrees (0.01 s) every other peak. The four peaks identify traces of tip vortex cavitating flows equably shedding from four blades, clearly reflecting blade frequency (100 Hz) of propeller which coincides with four-blade propeller with revolution speed n=25 r/s. Some discrepancies lie in amplitude of the peaks in a period because of small differences of the blades geometry and its grid. In addition, comparison of pressures evolutions in Figure 4 demonstrates increasing J with decreasing amplitude of pressure fluctuation due to the reduced propeller load. This result coincides with the experiment in ref. [10].

According to different radial positions, the slipstream of propeller wake is partitioned to three areas from inner (near hub) to outer (near tip), called hub vortex passage, blade sheet passage, and tip vortex passage. The correlation between pressures and flows structure is shown in Figure 5. The contour in Figure 5(a) is the axial velocity normalized by the free stream velocity, namely (U_X/U_∞) , in a longitudinal plane in the slipstream tube behind a blade. The main characteristics of flow structures in propeller wake, such as tip vortex, hub vortex and viscous wake flow shedding from the trailing edge of blades, are clearly displayed in the contour. Here, the accuracy of the computed axial velocity around r/R=0.9 is less than experimental result for the main reason that the number of grid cells in the region is not enough. In the axial plane of x/R=1.0, three radial positions (r/R=0.3, r/R=0.7, r/R=0.9) within the slipstream tube and another position (r/R=1.2) outside of the slipstream tube were used for investigation of pressure fluctuating in radial direction. The numerical predictions of pressure of the four positions indicate different features such as amplitude due to effect of flow structures. In Figure 5(c), the amplitude of pressure at r/R=0.3 near the hub passage is small due to strong influence of hub vortex. In Figure 5(d), the amplitude of pressure at r/R=0.7 becomes larger due to strong influences of low-pressure flow in blade sheet passage. In Figure 5(b), the amplitude of pressure at r/R=0.9 in the tip passage is the largest due to strong influence of tip vortex cavitation. The result indicates that the tip vortex cavitation is the most

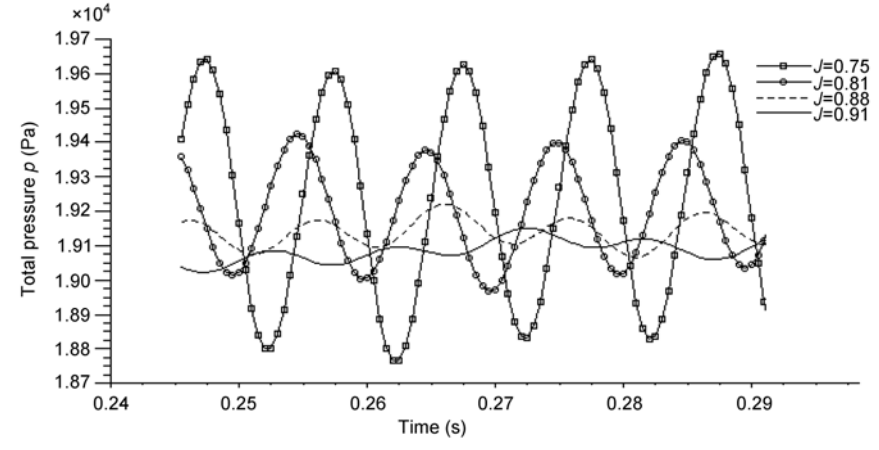


Figure 4 The total pressure at axial x=0.5R and radial r=0.9R.

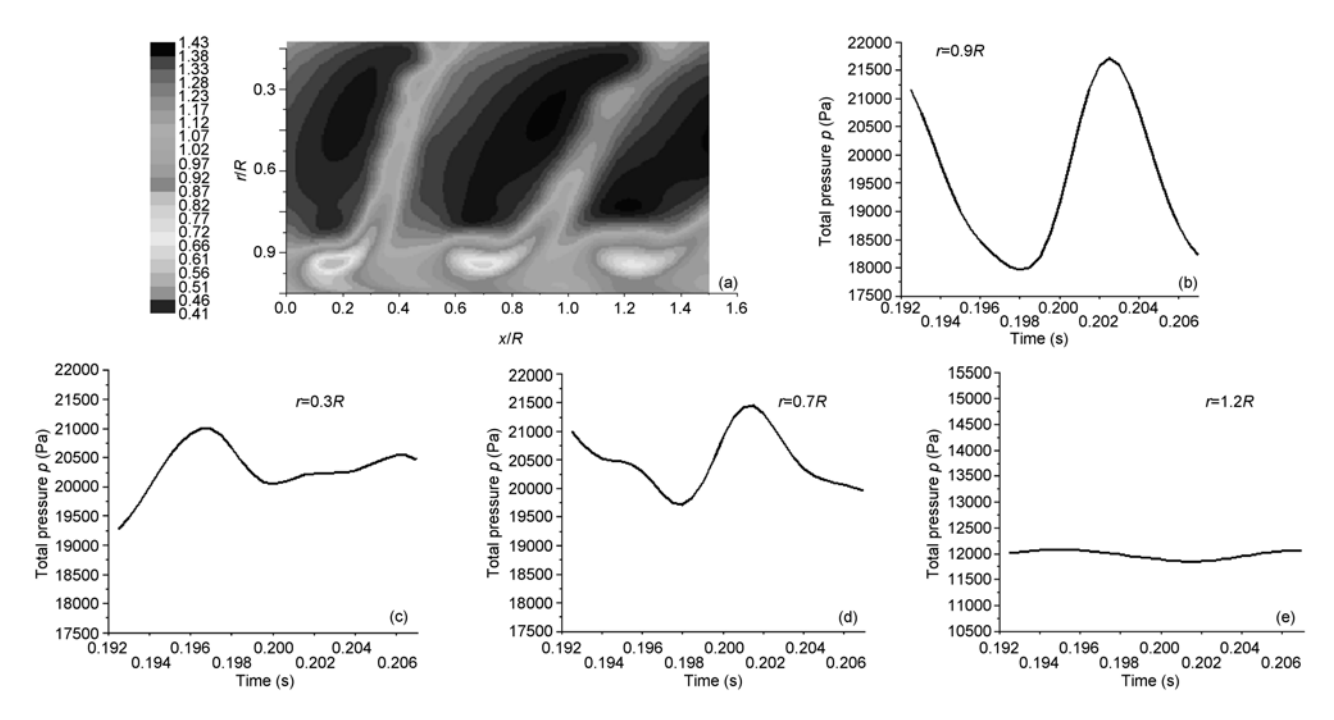


Figure 5 Numerical results of axial velocity and total pressure. (a) The normalized axial velocity in a longitudinal plane (U_X/U_∞) ; (b) the total pressure at x/R=1.0, r=0.9R; (c) the total pressure at x/R=1.0, r=0.3R; (d) the total pressure at x/R=1.0, r=0.7R; (e) the total pressure at x/R=1.0, r=0.2R.

important reason for the pressure fluctuation. In Figure 5(e), the amplitude of pressure at r/R=1.2 outside of the slipstream reduces clearly. At these radial positions close to trailing edge of propeller blade for axial position x/R=1.0, pressure spectra are based on blade frequency. All these results are in agreement with corresponding experiment [10].

For good comparison with corresponding experimental results, the conditions of J at 0.71, 0.88 and reference pressure at 26821 Pa, 101325 Pa are selected to numerically predict pressure fluctuation in wake. Further downstream in the transitional wake, the numerical predictions of pressure at four axial positions (x/R=1.5, x/R=2.0, x/R=3.0, x/R=4.0) with the same radial position (r/R=0.3) are shown in Figures 6 and 7. In the region, pressure varies clearly enough to indicate the feature of wake. The two predictions indicate that with the increasing distance from propeller disk, the number of pressure signal peaks becomes less in one period and discrepancies between amplitudes of peaks become larger. The results reflect frequency decreasing and instability of pressure signals amplitudes. The variations connect with the instability of slipstream tube in wake. Furthermore, compared with wave shapes at the condition of different J and the same axial position, it is generally found that the pressure at J=0.88 is more stable than that at J=0.71. The result indicates that with propeller load increasing and J decreasing, the wake starts to be unstable. At the same time, the unstable process occurs fast and becomes more close to propeller, which coincides with experimental conclusion [21]. In addition, the amplitude of pressure fluctuation decreases with diminishing J and increasing distance from propeller disk. The pressure evolutions in Figures 6 and 7 coincide with experiment data [9].

Figure 8 is the power spectral density of the pressure signals in Figures 6 and 7, clearly reflecting frequency evolution. In the figure, all the spectra are based on blade frequency at x=1.5R. According to two groups data in Figures 8(a) and 8(b), the former shows a visible peak of shaft frequency (25 Hz) at x=3R, and a strong peak of shaft frequency at x=4R, while the later shows a weak peak of shaft frequency at x=3R, and a visible peak of shaft frequency. At the same time, from Figures 8(c) and 8(d), the former shows a strong peak of shaft frequency at x=2R, while the later shows shaft frequency at x=2R, and a visible peak of shaft frequency at x=3R. The results above illustrate that in the wake passage near hub (r/R=0.3) the transformation of blade frequency to shaft frequency becomes fast with the decreasing J. In addition, from Figures 8(a) and 8(c), the former shows a visible peak of shaft frequency at x=3R, while the later shows a strong peak of shaft frequency at x=2R. At the same time, from Figures 8(b) and 8(d), the former shows a visible peak of shaft frequency at x=4R, while the later shows a visible peak of shaft frequency at x=3R. The results above indicate that the frequency transformation becomes fast with decreasing reference pressure, namely cavitation number. The characteristic of frequency evolution reflects the instability process of forming mechanism of pressure in wake. The instability strictly relates to

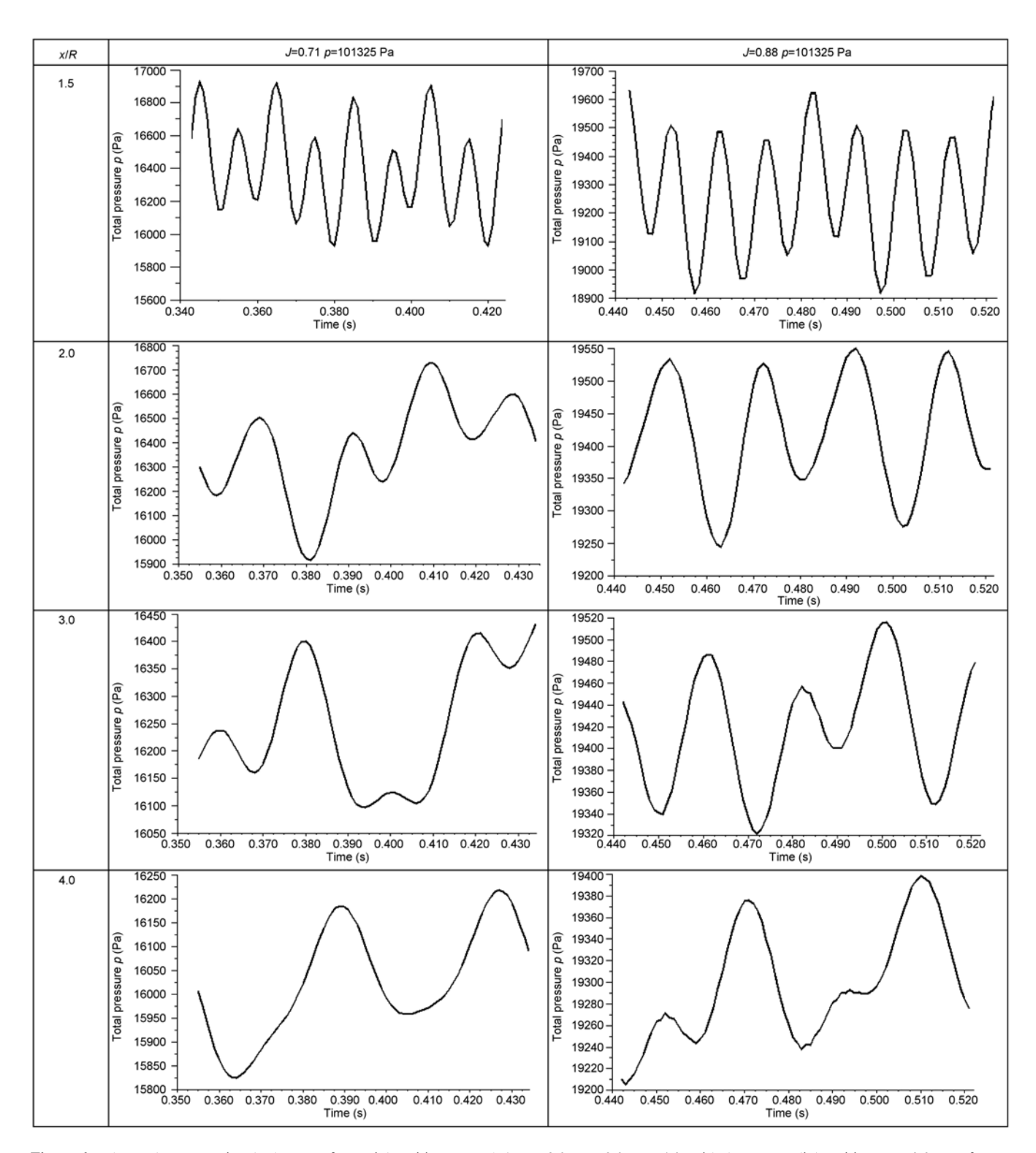


Figure 6 The total pressure signals shapes at four axial positions (x/R=1.5, x/R=2.0, x/R=3.0, x/R=4.0) with the same radial position (x/R=0.3) at reference pressure p=101325 Pa.

the interaction between the tip vortex and blade sheet wake of the next blade [22]. The amplitude of power spectral density at J=0.88 is obviously smaller than that at J=0.71,

reflecting lower propeller load at J=0.88. The characteristic analysis of pressure fluctuation above involves the transitional wake. For the far wake, the prediction is difficult due

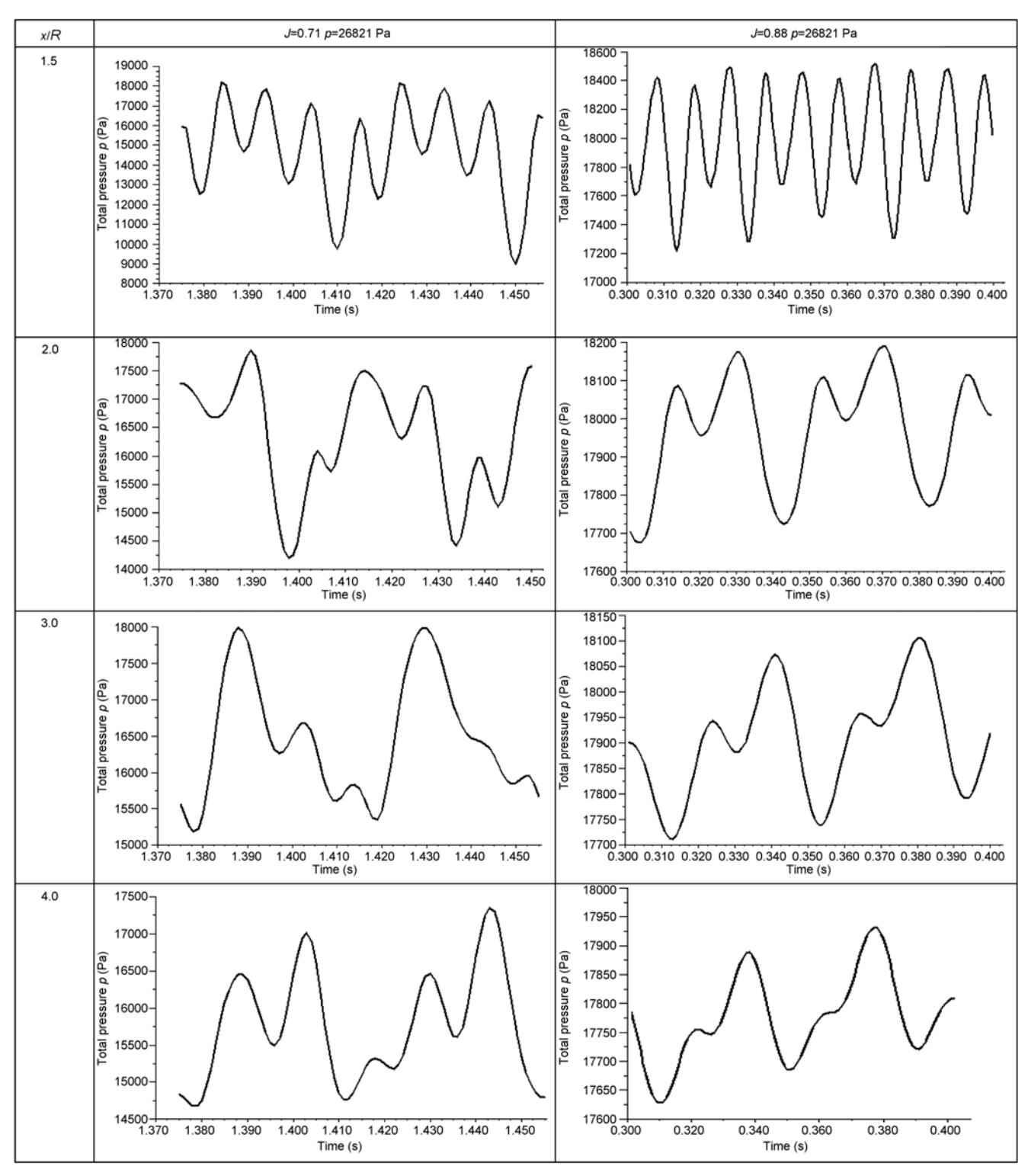


Figure 7 The total pressure signals shapes at four axial positions (x/R=1.5, x/R=2.0, x/R=3.0, x/R=4.0) with the same radial position (r/R=0.3) at reference pressure p=26821 Pa.

to larger size of grid cells in the region.

5 Conclusion

In the present study, the two important forming mechanisms

of cavitation noise, namely cavitation and wake field behind a ship propeller, are investigated. Comparing the measured data [10,20] with numerical data generated by the modified cavitation model and turbulence model, we draw some conclusions. (1) Based on good prediction of sheet cavitation, the prediction of the tip vortex cavitation and hub vortex

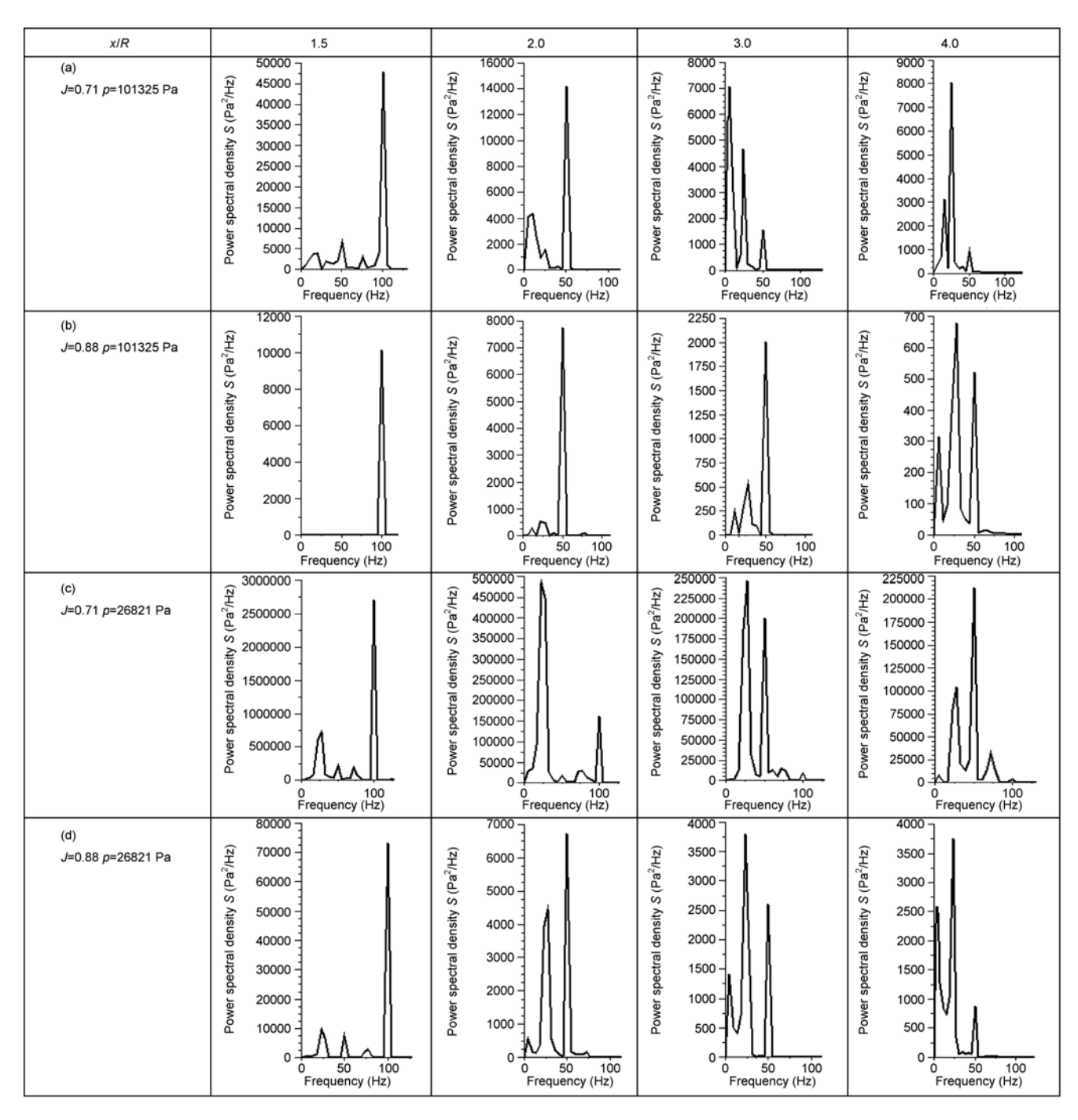


Figure 8 The power spectral density of pressure.

cavitation is performed, which is rarely reported in other literature. (2) For the prediction of pressure in wake, the shaft and blade frequency accords with propeller model and parameters. The axial velocity in longitudinal plane is not well predicted, but can denote the structure of wake flow. (3) The amplitude of pressure at r/R=0.9 in the tip passage is the largest, indicating that the tip vortex cavitation is the most important resource of the pressure fluctuation. Depending on these correct predictions, we further investigate numerical features of spectra and wave shape of pressure in wake at

different J and reference pressure conditions and get other conclusions. (1) The amplitude of pressure fluctuation decreases with increasing J reflecting load decreased. (2) With increasing distance from propeller disk, the pressure varies clearly. The blade frequency is gradually lost, and replaced by the shaft frequency, illustrating instability of wake. The translation becomes faster with decreasing J and cavitation number. However, the tip vortex cavitation is not well predicted mainly due to the limited knowledge to mathematics model of cavitation. In addition, for the grid dependence

study, through comparison of the computed results of several grids with different meshing strategies, we find out that error of propeller geometric model and grids can have an influence on the computed results. Compared with the structured grids, the unstructured grids affect the prediction of location and degree of cavitation. For the same meshing strategy, the density of cells has little influence on the prediction of location of sheet cavitation, but has influence on prediction of sheet cavitation degree, unsteady velocity and pressure field.

This work was supported by the Pre-research Major Project of China (Grant No. 06904002068).

- 1 Lee C. Prediction of steady and unsteady performance of marine propellers with or without cavitation by numerical lifting surface theory. Ph.D. Dissertation. Cambridge, MA: Department of Ocean Engineering of Massachusetts Institute of Technology, 1979
- 2 Ye J M. Predicting pressure fluctuations on ship hulls due to intermittently cavitating propellers. J Ship Mech, 2005, 9(6): 21–29
- 3 Ding S T, Tang D H, Zhou W X, Panel method of CSSRC for propeller in steady flows (in Chinese). J Ship Mechs, 2005, 9(5): 46–60
- 4 Fu H P, Li F X. A numerical analysis of the flow around a partially-cavitating axisymmetric body (in Chinese). Acta Mech Sin, 2002, 34(2): 278–285
- 5 Streckwall H, TiggesK. Numerical propulsion for podded propeller driven ship. The 15th International Conference on Hydrodynamics in Ship Design Safety and Operation. Gdansk, Poland, 2003
- 6 Liu S H, Shao J, Wu S F, et al. Uumerical simulation of pressure fluctuation in Kaplan turbine. Sci China Ser E-Tech Sci (in Chinese), 2009, 39(4): 626–634
- 7 Matevz D, Rudolf B, Bernd S, et al. Experimental evaluation of numerical simulation of cavitating flow around hydrofoil. Eur J Mech B/Fluids, 2005, 24: 522–538
- 8 Jules W, David A, Richard B, et al. Propeller cavitation breakdown analysis. ASME J Fluid Eng, 2005, 127: 995–1002
- 9 Shin H R, Takafumi K. Propeller cavitation study using an unstruc-

- tured grid based Navier-Stokes Solver. ASME J Fluids Eng, 2005, 127: 986-994
- Mario F, Fabio D F. Analysis of the propeller wake evolution by pressure and velocity phase measurements. Exp Fluids, 2006, 41: 441–451
- Ashok K S, Mahesh M A, Li H Y, et al. Mathematical basis and validation of the full cavitation model. ASME J Fluids Eng, 2002, 124(3): 617–624
- 12 Kubota A, Kato H. A new modeling of cavitating flows: A numerical study of unsteady cavitation on a hydrofoil section. J Fluid Mech, 1992, 240: 59–96
- 13 Brennen C E. Cavitation and Bubble Dynamics. Oxford: Oxford University Press, 1995
- 14 Markatos N C, Singal A K. Numerical analysis of one-dimensional, two-phase flow a vertical cylindrical pump. Adv Eng Software, 1982, 4(3): 99–106
- Yakhot V, Orszag S A. Renormalized group analysis of turbulence: I. basic theory. J Sci Comput, 1986, 1: 3–5
- 16 Orszag S A, Yakhot V. Renormalization Group Modeling and Turbulence Simulations, Near Wall Turbulent Flows. Amsterdam: Elsevier, 1993
- 17 Coutier-Delgosha O, Reboud J L, Delannoy Y. Numerical simulation of the unsteady behavior of cavitating flows. Int J Numer Meth Fluids, 2003, 42: 527–548
- Franciso P, Francesco S, Fabio D F, et al. Experimental and numerical investigation of the cavitation pattern on a marine propeller. 24th Symposium on Naval Hydrodynamics, Fukuoka, Japan, 8–13 July, 2002
- 19 Zhu Z F, Fang S L, Wang X Y. Propeller cavitation research using an unstructured grid based RANS Solver (in Chinese). Ocean Eng, 2009, 24(4): 103–107
- 20 Francesco S, Claudio T, Luca G, A viscous/inviscid coupled formulation for unteady sheet cavitation modelling of marine profellers. Fifth International Symposium on Cavitation (CAV2003), Osaka, Japan, November 1–4, 2003. 1–16
- 21 Di F F, Di F D, Felli M, et al. Experimental investigation of the propeller wake at different loading condition by PIV. J Ship Res, 2004, 48 (2): 168–190
- 22 Mario F, Giulio G, Roberto C. Effect of the number of blades on propeller wake evolution. Exp Fluids, 2008, 44: 409–418